

Direct observation of dynamic surface acoustic wave controlled carrier injection into single quantum posts using phase-resolved optical spectroscopy

S. Völkl,¹ F. Knall,¹ F. J. R. Schüle,¹ T. A. Truong,² H. Kim,³ P. M. Petroff,² A. Wixforth,¹ and H. J. Krenner^{1, a)}

¹⁾*Lehrstuhl für Experimentalphysik 1 and Augsburg Centre for Innovative Technologies (ACIT), Universität Augsburg, 86159 Augsburg, Germany*

²⁾*Materials Department, University of California, Santa Barbara CA 93106, United States*

³⁾*Physics Department, University of California, Santa Barbara CA 93106, United States*

A versatile stroboscopic technique based on active phase-locking of a surface acoustic wave to picosecond laser pulses is used to monitor dynamic acoustoelectric effects. Time-integrated multi-channel detection is applied to probe the modulation of the emission of a quantum well for different frequencies of the surface acoustic wave. For quantum posts we resolve dynamically controlled generation of neutral and charged excitons and preferential injection of holes into localized states within the nanostructure.

PACS numbers: 71.35.-y, 77.65.Dg, 78.55.Cr, 78.67.Hc

Keywords: quantum dot, quantum post, surface acoustic wave, carrier injection

^{a)}Electronic mail: hubert.krenner@physik.uni-augsburg.de

Surface acoustic waves (SAWs) are a powerful tool for the investigation of electrically and optically active low-dimensional semiconductor structures at frequencies exceeding several GHz. For optically active structures, examples range from acoustic charge and spin transport^{1,2} to the manipulation of optical resonances in quantum dots (QDs)^{3,4} and optical cavities⁵. Due to the high frequencies involved, these optical experiments require a high temporal resolution. This is typically achieved by using single-channel time-correlated single photon counting techniques or high speed, intensified charge coupled device (iCCD) detectors or streak cameras which have, however, relatively poor sensitivity^{3,4,6}.

In this letter, we demonstrate *dynamic* acoustically controlled carrier injection into the confined levels of self-assembled quantum posts (QPs)⁷ and the dynamic modulation of the photoluminescence (PL) emission of a quantum well (QW) using an easy to implement stroboscopic technique in which a picosecond diode laser is phase-locked to the SAW. Compared to conventional schemes our technique allows for a fully time-integrated multi-channel detection with a phase resolution limited by the radiative lifetime of the emitter system, only. For our experiments, we use a sample containing a single layer of 23 nm high QPs grown by molecular beam epitaxy⁸. These QPs are columnar nanostructures embedded in a lateral matrix QW as shown in Fig. 1 (a) in which hole states are localized at the two ends as indicated in the sketched valence band. Details on the applied growth technique using a stacking sequence, the basic optical properties and device applications of QPs are described elsewhere⁹. For device processing we select a region with a sufficiently low surface density ($< 1 \mu\text{m}^{-2}$) of QPs where we can probe (i) individual QPs and (ii) the lateral matrix QW surrounding the QPs. On this sample a set of lithographically defined interdigital transducers (IDTs) allow for SAW excitation at frequencies of $f_1 = 232.2$ MHz, $f_2 = 538.3$ MHz and $f_3 = 968.5$ MHz at low temperatures, respectively.

We study the emission of these QPs and the lateral QW⁸ by conventional low temperature ($T \sim 10$ K) μ -PL. Carriers are photogenerated in the GaAs bulk using a diode laser emitting $\tau_{laser} \lesssim 100$ ps long pulses at $\lambda = 661$ nm focused to a $\sim 3 \mu\text{m}$ spot using a $50\times$ microscope objective. The signal is collected via the same lens and detected using a 0.5 m imaging grating monochromator and a highly sensitive, liquid nitrogen cooled, Si CCD camera. The excitation laser can be triggered either by an internal clock or using an external signal used for synchronization with the RF signal applied to the IDTs to generate a SAW. In the experiments presented here, the SAW is applied in pulses (on/off duty cycle 1:9,

53 $f_{rep} \sim 100$ kHz). As shown in Fig. 1 (b) the excitation laser pulses can be phase-locked for
 54 the SAW frequency being an harmonic of the laser repetition rate: $f_{SAW} = n \cdot f_{laser}$. Under
 55 these conditions the short laser pulse is exciting the sample at a constant phase ϕ i.e. fixed
 56 time of the SAW oscillation. The full SAW cycle can then be resolved by variation of the
 57 phase offset $\Delta\phi$ between the SAW and the train of laser pulses. This is shown for $\Delta\phi = 180^\circ$
 58 for the solid black and red (gray) laser pulses in Fig. 1 (b). Thus, for a sufficiently fast
 59 radiative process with a PL decay time constant $\tau_{PL} \cdot f_{SAW} < 1/2$, we are able to obtain *full*
 60 phase information. Moreover, simply by choosing an arbitrary phase relation [dashed laser
 61 pulses in Fig. 1 (b)], phase-averaged spectra are recorded.

62 To study the phase and thus temporal resolution of this technique, we start by investigat-
 63 ing the dynamic quenching of the matrix QW PL for different f_{SAW} ⁷. We actively lock the
 64 laser pulses to the SAW by setting $n = 3, 7, 13$ for f_1, f_2 and f_3 , respectively. To achieve
 65 comparable experimental conditions, we applied RF powers for which a similar suppression
 66 of the PL was observed for these frequencies. As we tune ϕ , [c.f. Fig. 2] we observe a clear
 67 oscillatory behavior of the normalized QW emission intensity (I/I_0 , symbols) arising from
 68 the dynamic modulation of band edges which are well reproduced by fitting sine functions
 69 with the period of the SAW (lines) and agrees well with previous work⁶. The absolute
 70 value of ϕ depends on the distance of the laser spot to the IDT which leads to the finite
 71 offset for the two frequencies and the data on QPs presented later. The amplitude (A/I_0)
 72 of this oscillation is significantly reduced for the higher frequency since the time between
 73 the maximum and minimum SAW amplitude given by $1/(2 \cdot f_2) = 0.93$ ns is shorter than
 74 the radiative decay time of the QW $\tau_{PL} = 1.25$ ns. This is further confirmed by a detailed
 75 analysis of A/I_0 as a function of the suppression of the QW PL ($1 - I/I_0$) for f_1 and f_2 shown
 76 as an inset of Fig. 2. For the highest frequency (f_3) no more modulation is observed (data
 77 not shown). Thus, our stroboscopic technique can be readily applied to resolve periodically
 78 driven processes for radiative processes with $\tau_{PL} \cdot f_{SAW} \lesssim 1/2$.

80 We also applied the technique to QPs to monitor the dynamic sequential carrier injec-
 81 tion controlled by a SAW ($f_1 = 232.2$ MHz). These nanostructures are particularly suited
 82 due to the efficient acoustic charge conveyance in the lateral matrix QW. In Fig. 3 (a)
 83 we present SAW phase-averaged PL spectra recorded under weak optical pumping from
 84 an individual QP as a function of the applied RF power (grayscale representation). We
 85 observe a characteristic switching⁷ from an emission doublet arising from recombination
 86

87 of the negatively charged exciton ($1X_{l,h}^-$) to a doublet at higher energies assigned to the
 88 charge neutral single exciton ($1X_{l,h}^0$). The indices l (h) denote the lower (higher) energy
 89 line of the doublet. These doublets arise from recombinations between *delocalized* electrons
 90 and the two non-degenerate hole levels¹⁰ at the two ends of the QP [c.f. Fig. 1 (a)]. We
 91 performed full SAW phase scans at the two characteristic power levels marked in Fig. 3
 92 (a): $P_1 = -1$ dBm is close to the onset of charge conveyance and the emission spectra is
 93 dominated by emission of $1X_{l,h}^-$. At $P_2 = +8$ dBm, efficient charge conveyance occurs, the
 94 $1X_{l,h}^-$ PL lines are strongly suppressed and emission of $1X_{l,h}^0$ is detected. Under the applied
 95 experimental conditions the band gap modulation induced by the SAW⁶ is not sufficient to
 96 *spectrally tune* individual PL lines^{3,7}. In Fig. 3 (b) we compare the $1X_{l,h}^0$ doublet at P_2
 97 for two distinct relative SAW phases split by $\Delta\phi = 180^\circ$. For $\phi = 60^\circ$ (gray shaded) the
 98 lower energy line $1X_l^0$ of the doublet is more intense than $1X_h^0$ whilst for $\phi = 240^\circ$ (line)
 99 both lines have approximately the same intensity. Since the two lines of the doublet arise
 100 from localization of holes at either the upper or the lower end of the QP, this observation
 101 demonstrates that the injection of this carrier species into the QPs also depends on the local
 102 ϕ .

103
 104 The detailed investigation of the SAW controlled carrier capture and a complete analysis
 105 of the relative PL intensities of different excitonic species and emission doublets is presented
 106 in Fig. 4. We plot the relative intensities of $1X^0$ and $1X^-$, I_{1X^0}/I_{1X^-} as a function of the
 107 local SAW phase in Fig. 4 (a) and (c) and the relative intensities of the two lines forming the
 108 emission doublets, I_{1X_h}/I_{1X_l} , in Fig. 4 (b) and (d) at both power levels (P_1 diamonds, P_2
 109 circles). Clearly, all ratios show the same oscillatory behavior as a function of ϕ , providing
 110 direct evidence for dynamic carrier capture directly controlled by the SAW. In particular,
 111 within this range of SAW powers the generation of charged and neutral excitons is highly
 112 dependent on ϕ . This follows from our observation that the relative intensity detected from
 113 the $1X_{l,h}^0$ is reduced by a factor of 2 at $\phi_0 = 80^\circ$ compared to $\phi_0 + 180^\circ$ [c.f. Fig. 4 (a)].
 114 As can be seen from both experimental data (symbols) and the fits (lines), at both power
 115 levels [c.f. Fig. 4 (a) and (f)] the maxima occur at almost identical ϕ indicating the same
 116 driving mechanism in both cases. The SAW induces an Type-II band edge modulation
 117 giving rise to local accumulation of electrons or holes¹¹ at distinct values of ϕ_{SAW} as shown
 118 schematically in Fig. 4 (e) and (f). At ϕ_0 an attractive minimum is formed for electrons

in the conduction band while the situation is inverted at $\phi_0 + 180^\circ$ and holes are accumulated at a stable maximum in the valence band. Thus, the local concentration of the two carrier species is dynamically controlled locally by ϕ leading to the observed modulation of the QP occupancy. From the relative intensity of I_{1X^0}/I_{1X^-} we conclude that (i) $1X^-$ is predominantly formed around ϕ_0 where electrons are collected at the position of the QP whilst (ii) a local accumulation of holes is required to form $1X^0$. The finite phase-shift between P_1 and P_2 [c.f. Fig 4 (a) and (c)] could arise from contributions between lateral and vertical piezoelectric fields. Furthermore, we investigated in detail the modulation with the emission doublet $1X_{h,l}$. For both $1X^0$ and $1X^-$, the same phase dependence of the ratio of the energetically higher $1X_h$ and the lower $1X_l$ line is observed in the experimental data (symbols) with the corresponding fits (lines) in Fig. 4 (b) and (d). Moreover, the intensity of $1X_h$ is increased by about a factor of 2 at $\phi_0 + 180^\circ$ compared to ϕ_0 . This finding indicates that at these distinct phases the hole is injected predominantly at one specific end of the QP. The preferential injection could be driven by the vertical electric field component at these local SAW phases. This finite electric field gives rise to an enhanced hole localization at one side of the lateral QW leading to an increase in the population of the corresponding localized hole level in the QP. This interpretation is in good agreement with the observed localization (delocalization) of holes (electrons) within the QP for weak static vertical electric fields^{10,12}. Since the oscillation of $1X_h$ and $1X_l$ are in phase for both exciton species we conclude that the major contribution to the energetic splitting within the doublet indeed arises from the distinct single particle energies of the localized hole states at the two ends of the QP.

In summary, we demonstrated an stroboscopic technique to probe the influence of a SAW on optical emitters using time-integrated multi-channel detection based on active phase-locking of a SAW to the excitation laser pulses. It can be applied to monitor the dynamic modulation of the emission of a QW and the dynamic SAW controlled injection of carriers into the confined levels of QPs. Our versatile technique is limited only by the radiative lifetime of the studied system and can be readily applied to investigate a wide range of optically active nanosystems such as different types of single and coupled QDs^{3,4,13}, microcavities^{5,14} or nanostructures directly transferred onto piezoelectric substrates¹⁵.

This work was supported by the *Nanosystems Initiative Munich* (NIM), NSF via NIRT

(CCF- 0507295), DARPA SEEDLING and the Humboldt-Foundation.

REFERENCES

- ¹C. Rocke, S. Zimmermann, A. Wixforth, J. P. Kotthaus, G. Böhm, and G. Weimann, Phys. Rev. Lett. **78**, 4099 (1997).
- ²M. Rotter, A. V. Kalameitsev, A. O. Govorov, W. Ruile, and A. Wixforth, Phys. Rev. Lett. **82**, 2171 (1999); T. Sogawa, P. V. Santos, S. K. Zhang, S. Eshlaghi, A. D. Wieck, and K. H. Ploog, Phys. Rev. Lett. **87**, 276601 (2001).
- ³J. R. Gell, M. B. Ward, R. J. Young, R. M. Stevenson, P. Atkinson, D. Anderson, G. A. C. Jones, D. A. Ritchie, and A. J. Shields, Appl. Phys. Lett. **93**, 081115 (2008).
- ⁴O. D. D. Couto, S. Lazić, F. Iikawa, J. A. H. Stotz, U. Jahn, R. Hey, and P. V. Santos, Nat. Photon. **3**, 645 (2009); M. Metcalfe, S. M. Carr, A. Muller, G. S. Solomon, and J. Lawall, Phys. Rev. Lett. **105**, 037401 (2010).
- ⁵M. M. de Lima Jr. and P. V. Santos, Rep. Prog. Phys. **68**, 1639 (2005).
- ⁶F. Alsina, P. V. Santos, R. Hey, A. García-Cristóbal, and A. Cantarero, Phys. Rev. B **64**, 041304(R) (2001); T. Sogawa, H. Sanada, H. Gotoh, H. Yamaguchi, S. Miyashita, and P. V. Santos, Appl. Phys. Lett. **94**, 131912 (2009).
- ⁷S. Völkl, F. J. R. Schüle, F. Knall, D. Reuter, A. D. Wieck, T. A. Truong, H. Kim, P. M. Petroff, A. Wixforth, and H. J. Krenner, Nano Lett. **10**, 3399 (2010).
- ⁸J. He, H. J. Krenner, C. Pryor, J. P. Zhang, Y. Wu, D. G. Allen, C. M. Morris, M. S. Sherwin, and P. M. Petroff, Nano Lett. **7**, 802 (2007); L. H. Li, G. Patriarche, and A. Fiore, J. Appl. Phys. **104**, 113522 (2008).
- ⁹H. J. Krenner and P. M. Petroff, Solid State Commun. **149**, 1386 (2009); P. Ridha, L. H. Li, M. Mexis, P. M. Smowton, J. Andrzejewski, G. Sek, J. Misiewicz, E. P. O'Reilly, G. Patriarche, and A. Fiore, IEEE J. Quantum Electron. **46**, 197 (2010).
- ¹⁰H. J. Krenner, C. Pryor, J. He, J. P. Zhang, Y. Wu, C. M. Morris, M. S. Sherwin, and P. M. Petroff, Physica E **40**, 1785 (2008), arXiv:0709.2392 [cond-mat.mtrl-sci].
- ¹¹F. Alsina, P. V. Santos, H.-P. Schönherr, W. Seidel, K. H. Ploog, and R. Nötzel, Phys. Rev. B **66**, 165330 (2002).
- ¹²H. J. Krenner, C. E. Pryor, J. He, and P. M. Petroff, Nano Lett. **8**, 1750 (2008).
- ¹³F. J. R. Schüle, A. Laucht, J. Riikonen, M. Mattila, M. Sopanen, H. Lipsanen, J. J.

181 Finley, A. Wixforth, and H. J. Krenner, Appl. Phys. Lett. **95**, 083122 (2009); H. J.
182 Krenner, S. Stuffer, M. Sabathil, E. C. Clark, P. Ester, M. Bichler, G. Abstreiter, J. J.
183 Finley, and A. Zrenner, New J. Phys. **7**, 184 (2005).

184 ¹⁴N. G. Stoltz, M. Rakher, S. Strauf, A. Badolato, D. D. Lofgreen, P. M. Petroff, L. A. Col-
185 dren, and D. Bouwmeester, Appl. Phys. Lett. **87**, 031105 (2005); A. Kress, F. Hofbauer,
186 N. Reinelt, M. Kaniber, H. J. Krenner, R. Meyer, G. Böhm, and J. J. Finley, Phys. Rev.
187 B **71**, 241304 (2005).

188 ¹⁵V. I. Talyanskii, D. S. Novikov, B. D. Simons, and L. S. Levitov, Phys. Rev. Lett. **87**,
189 276802 (2001); M. P. V. Kouwen, M. E. Reimer, A. W. Hidma, M. H. M. van Weert,
190 R. E. Algra, E. P. A. M. Bakkers, L. P. Kouwenhoven, and V. Zwiller, Nano Lett. **10**,
191 1817 (2010); D. A. Fuhrmann, H. J. Krenner, A. Wixforth, A. Curran, K. A. Prior, R. J.
192 Warburton, and J. Ebbecke, J. Appl. Phys. **107**, 093717 (2010).

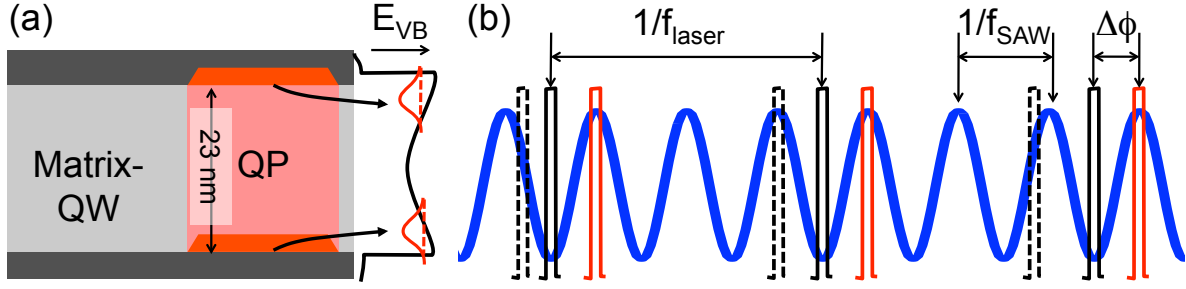


FIG. 1. (Color online) (a) Schematic of self-assembled QPs embedded in a lateral matrix QW and localization of holes in local valence band minima at ends of the QP. (b) Scheme to active locking and tuning (solid) of the SAW (bold) phase and the laser pulses (solid) or averaging over all phases (dashed).

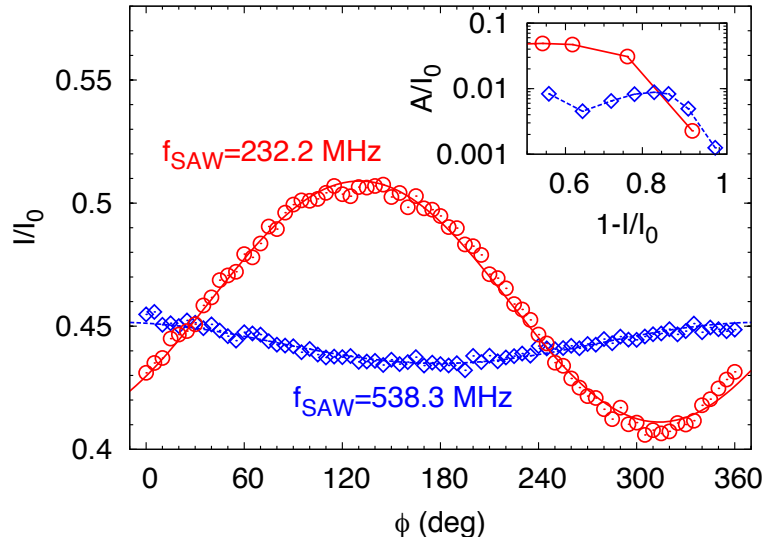


FIG. 2. (Color online) Main panel: Integrated and normalized QW emission (symbols) and sine fits (lines) for SAW frequencies f_1 (circles) and f_2 (diamonds) as a function of the local phase ϕ . Inset: Relative amplitude of the oscillation for different levels of SAW induced emission quenching ($1 - I/I_0$).

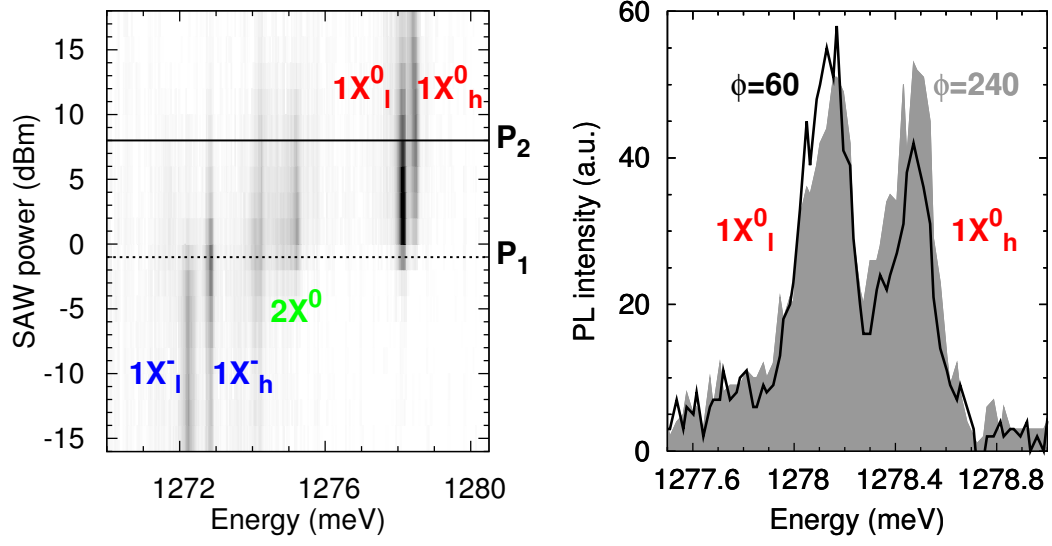


FIG. 3. (Color online) (a) Phase-averaged, RF-power dependent PL of a single QP for f_1 plotted in grayscale representation. Switching between $(1X_{h,l}^-)$ and $(1X_{h,l}^0)$ occurs at $P_1 = -1$ dBm. (b) Emission of $1X_{h,l}^0$ at P_2 for $\phi = 60^\circ$ and 240° showing a pronounced modulation of the doublet.

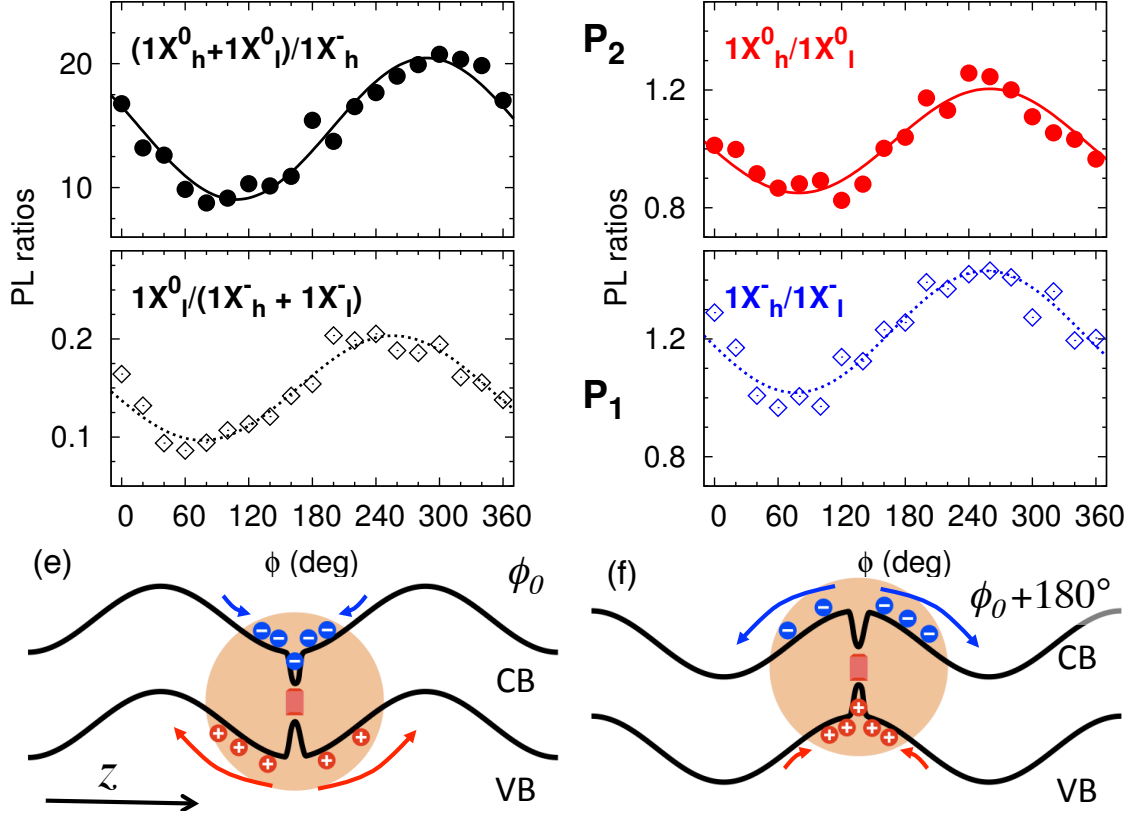


FIG. 4. (Color online) Relative intensities (symbols) of $1X^0$ and $1X^-$ (a) and (c) and $1X_{h,l}$ doublets (b) and (d) for a f_1 at P_1 (lower panels) and P_2 (upper panels) as a function of ϕ . The corresponding fits are plotted as lines. (e) and (f) SAW-induced band edge modulation: At $\phi_0 = 80^\circ$ and $\phi_0 + 180^\circ$ attractive potentials for electrons and holes are locally induced by the SAW at the QP position.